IEEE Access
Multidisciplinary | Rapid Review | Open Access Journal

Received November 7, 2020, accepted November 27, 2020, date of publication December 7, 2020,
date of current version December 18, 2020.

Digital Object Identifier 10.1109/ACCESS.2020.3043055

Evaluation of an Optimal Radial-Loop Configuration for a Distribution Network With PV Systems to Minimize Power Loss

AKIHISA KANEKO[1], (Graduate Student Member, IEEE), YASUHIRO HAYASHI[1], (Member, IEEE), TAKAYA ANEGAWA[2], HIDEYASU HOKAZONO[2], AND YUKIYASU KUWASHITA[2]

[1]Department of Electrical Engineering and Bioscience, Waseda University, Tokyo 169-8555, Japan
[2]Kansai Transmission and Distribution, Inc., Osaka 530-0005, Japan

Corresponding author: Akihisa Kaneko (a-kaneko.0811@fuji.waseda.jp)

ABSTRACT This paper proposes a method to determine an optimal radial-loop configuration to minimize power loss in a distribution network with photovoltaic (PV) systems and evaluates the effectiveness of this configuration. Due to the disaggregation of transmission and distribution in a deregulated power system, stable and efficient operations in terms of voltage regulation and power loss reduction utilizing existing equipment is becoming more important for distribution system operators (DSOs). Japanese DSOs operate distribution networks in a radial configuration while supplying power to customers with high reliability. One method to reduce further power loss is to upgrade the network topology to a radial-loop configuration, which achieves partial loop structures by closing the tie-switches of the radial configuration. To implement a radial-loop configuration, DSOs must first evaluate the reliability, as a loop configuration can cause a feeder circuit breaker (FCB) malfunction and an expansion of the nonsupplied area during fault conditions. However, the impact of a radial-loop configuration on reliability and effectiveness has not been verified. Therefore, this paper proposes a method to determine an optimal radial-loop configuration that minimizes active power loss and maintains high reliability. In a numerical simulation, the reliability of radial-loop configurations is verified, and the effectiveness of the configuration is analyzed in terms of active power loss and voltage regulation under several PV system penetration conditions. A 6.6 kV distribution network consisting of 6 feeders and 11 tie-switches is modeled based on an existing Japanese distribution network and used for numerical simulation.

INDEX TERMS Radial-loop configuration for distribution network, active power loss, tie-switches status, detection of fault current by feeder circuit breaker, nonsupplied area under fault, voltage regulation, photovoltaic systems.

I. INTRODUCTION

Distribution system operators (DSOs) have taken various operational steps to ensure a stable and reliable power supply to customers while considering economic efficiency. In particular, the network configuration, which is defined as a set of the closed/open statuses of section switches (switches) and tie-switches, is an important foundation [1].

Recently, the increase in photovoltaic (PV) system penetration in the distribution network has caused voltage violations from the proper range. DSOs are required to clear voltage violations to improve supply reliability without curtailing PV system generation [2]. The clearing of voltage violations is an urgent issue for DSOs because the penetration of PV systems increasingly achieves the goals of the Paris agreement [3]. Due to the disaggregation of transmission and distribution in a deregulated power system, DSOs are required to solve network problems using existing equipment and do not depend on the control of generators [4]–[6]. Furthermore, the importance of minimizing power loss is increasing in terms of economic efficiency.

From this background, the methods used to determine an optimal network configuration have been widely discussed as referenced below because network reconfiguration can

The associate editor coordinating the review of this manuscript and approving it for publication was N. Prabaharan.

address voltage violations and reduce power losses simultaneously. Two main options exist for network configurations, namely, a radial configuration and a loop configuration. Many papers have discussed methods for an optimal radial configuration [7]–[25]. This configuration has been determined based on power loss, voltage deviation and load balance under normal conditions [7]–[15]. Several papers have considered indices in fault conditions, such as average energy not supplied (AENS) [16]–[25]. A study [14] analyzed the effectiveness of an hourly reconfiguration corresponding to output from renewable energy sources. In [7] and [25], cooperation schemes with electric vehicles were discussed.

On the other hand, loop configurations have not been widely considered due to concerns about the deterioration of supply reliability. However, these concerns have recently been addressed due to the development of optical communication technology and distribution automation systems [26]–[29]. Thus, several papers have focused on loop configurations as useful configurations for a future power system because this configuration can contribute to mitigating voltage violations and reducing power losses by balancing the power flow in feeders with distributed generators (DGs) [30]–[47]. In [30]–[38], new devices, such as a unified power flow controller or a loop power flow controller, were used for loop operations. In [30], the contribution from reducing voltage fluctuations was evaluated in a distribution network with DGs. The reconfiguration of a loop operation was discussed to maximize the hosting capacity of DGs [36]. To reduce the high expenses for new devices and distribution lines [32], [38], some studies verified the loop configuration by controlling only the existing switches [39]–[47]. For example, the increase in the hosting capacity of renewable energy and the reduction in power loss were evaluated using a distribution network model that referenced actual networks [39], [44]. Loop configurations were studied not only under normal conditions but also under fault conditions [32], [36], [45]. In [32], superconducting fault current limiters (SFCLs) were used to improve reliability in a loop configuration. In [45], the siting and sizing of DGs were optimized in a loop configuration by considering repairing fault periods (RFP). Therefore, the loop configuration needs to be determined by considering the power flow under normal conditions and by utilizing the existing equipment and systems under fault conditions.

The Japanese distribution network is one of the most reliable power systems in the world [48], [49]. This reliability is supported by two main systems: a sequential fault detection system and a distribution automation system (DAS) [28], [29]. The sequential fault detection system controls the status of switches after a fault occurs. The DAS then controls the switches and reconnects the feeder with an another bank to supply power to the nonfaulted areas. These systems are designed for a radial configuration. To ensure supply reliability, it is desirable that these systems are applied in the loop configuration. Thus, this paper focuses on a radial-loop configuration. This configuration creates partial loop structures by closing some tie-switches additionally in the base radial configuration. A tie-switch represents a switch connecting feeders within the same bank. DSOs can apply a radial-loop configuration to system operations easily because the DSOs change only the status of tie-switches in the base radial configuration, not all switches including section switches and tie-switches. For a radial-loop configuration, DSOs need to optimize the tie-switch status because the contribution to power loss reduction and the impact on the fault detection system, such as a malfunction of a feeder circuit breaker (FCB), depend on the location of closed tie-switches. The impact on the Japanese fault detection system and the effectiveness of the radial-loop configuration have not been evaluated. In particular, this effectiveness needs to be evaluated based on various indices, including the reduction of power loss, voltage regulation, and the transition of the optimal configuration under PV system penetration scenarios [42], [46], [50].

This paper proposes a method to determine the optimal radial-loop configuration by considering the supply reliability under the Japanese system. In the proposed method, the optimal configuration is determined to minimize active power loss while satisfying the constraints related to normal conditions, fault conditions and tie-switch status. Constraints related to normal conditions include node voltage and thermal capacity constraints. Constraints related to fault conditions include fault detection and the expansion of temporary non-supplied areas. In simulations, the impact on a fault detection system and the effectiveness of an active power loss reduction in a radial-loop configuration are evaluated using a 6.6 kV distribution network model with 6 feeders and 11 tie-switches. The optimal configuration is determined in 5 cases with different PV system penetration levels.

The major contributions of this paper include 1) evaluating the impact of using a radial-loop configuration on supply reliability, 2) proposing a method to determine an optimal network configuration by considering normal and fault conditions, and 3) evaluating the effectiveness of an optimal network configuration in terms of active power loss and voltage regulation under various PV penetration levels.

The rest of this paper is organized as follows. In Section II, the fault detection scheme in the Japanese system is explained, and concerns with using these systems in a radial-loop configuration are also addressed. In Section III, the proposed method for determining the optimal configuration is described and formulated. In Sections IV and V, the numerical simulation settings, the results and a discussion are presented, respectively. Finally, our concluding remarks are provided in Section VI.

II. FAULT DETECTION SCHEME IN JAPANESE SYSTEM

The Japanese distribution network utilizes switches that can be controlled remotely at high speed using optical fiber transmission [28], [29]. Supply reliability is improved by rapid fault detection and by restoring the power supply to nonfaulted sections by controlling these switches. The general

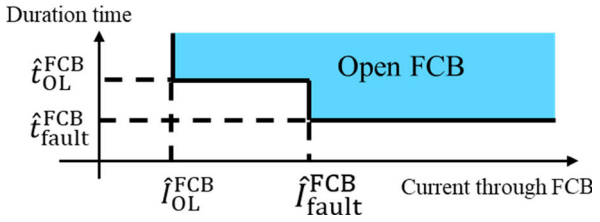

FIGURE 1. Condition under which the FCB needs to be opened. The FCB needs to be opened if the current through the FCB is stronger than $\hat{I}^{\mathrm{FCB}}_{\mathrm{fault}}$ to detect faults. Additionally, the FCB needs to be opened if the current through the FCB is stronger than $\hat{I}^{\mathrm{FCB}}_{\mathrm{OL}}$ to detect overloads.

scheme for dealing with a fault requires 2 steps: (a) detecting the fault current by a feeder circuit breaker (FCB) and opening the FCB and (b) identifying the fault section and supplying power to nonfaulted sections using a sequential fault detection system and a DAS. Section II describes the operational procedures in a radial configuration and their concerns under a radial-loop configuration.

A. DETECTION OF FAULT CURRENT BY FCB

To clear a ground fault or short-circuit fault properly, the FCB first needs to detect a fault current and open. Fig. 1 shows a condition for an FCB to open based on the current and duration time. If the current through the FCB is stronger than the threshold of fault current $\hat{I}^{\mathrm{FCB}}_{\mathrm{fault}}$ for the threshold duration time $\hat{t}^{\mathrm{FCB}}_{\mathrm{fault}}$, then the FCB is opened. Therefore, the threshold of fault current needs to be set as a lower value than the assumed fault current. Additionally, the FCB needs to be opened in case of an overload. The scheme for detecting an overload is the same as that for detecting a fault current. The parameters are the threshold of the current to detect an overload $\hat{I}^{\mathrm{FCB}}_{\mathrm{OL}}$ and the threshold of the duration time $\hat{t}^{\mathrm{FCB}}_{\mathrm{OL}}$. To properly detect the fault current and overload current by the FCB, $\hat{I}^{\mathrm{FCB}}_{\mathrm{fault}}$ needs to be set to a value larger than $\hat{I}^{\mathrm{FCB}}_{\mathrm{OL}}$, as given in Eq. (1),

$$\hat{I}^{\mathrm{FCB}}_{\mathrm{OL}} < \hat{I}^{\mathrm{FCB}}_{\mathrm{fault}}. \tag{1}$$

If this constraint is not satisfied, the FCB may open due to a malfunction during heavy power flow and not because of an overload. In this case, the supply reliability may deteriorate. Generally, $\hat{I}^{\mathrm{FCB}}_{\mathrm{OL}}$ is set by the product of the thermal capacity of the distribution line and a coefficient. DSOs need to select the network configurations by considering the parameter $\hat{I}^{\mathrm{FCB}}_{\mathrm{fault}}$.

In a radial-loop configuration, the current through an FCB may become small because the impedance from a fault point to the FCB increases by closing tie-switches. Therefore, the constraint given in Eq. (1) is more important.

B. SEQUENTIAL FAULT DETECTION SYSTEM

After the FCB opens, all the switches in the feeder are also opened. Then, a sequential fault detection system closes switches in sequence automatically to identify the fault section and to supply power to the nonfaulted sections. An overview of the procedure is shown in Fig. 2. Fig. 2 (a) shows the normal condition, where the feeder is divided into

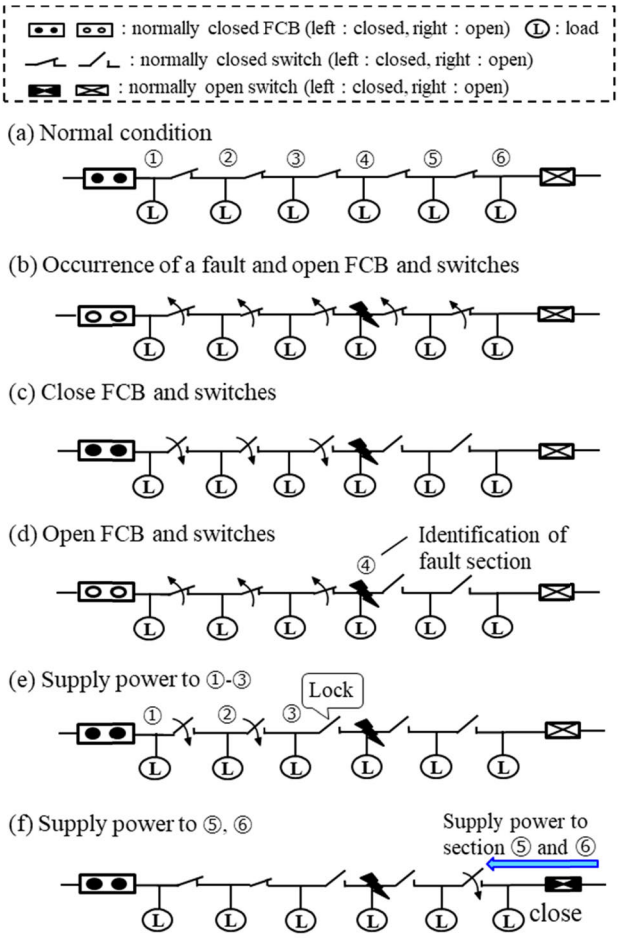

FIGURE 2. Procedure to detect fault sections and supply power to nonfaulted sections by the sequential fault detection system and the DAS. When the FCB detects a fault current, the FCB and all the switches open, and all loads are temporarily not supplied power in (b). Then, the fault section is detected by the switch controls in (c) and (d). Power is supplied to the load in nonfaulted sections by the switch controls in (e) and (f).

six sections by switches. In Fig. 2 (b), the FCB and all switches in the feeder are opened after a fault occurs. Then, the FCB and the switches are closed in sequence automatically to identify the fault section using the sequential fault detection system in Fig. 2 (c). When power is supplied to the fault section again, the FCB and all the switches are opened, and the fault section is identified, as shown in Fig. 2 (d). Then, the switches are closed to supply power to sections ①, ② and ③ in Fig. 2 (e). The sequential fault detection system performs these procedures automatically. Finally, the DAS closes the switch connecting with a feeder in another bank to supply power to the nonfaulted section at the end of the feeder in Fig 2 (f).

To apply these procedures in a radial-loop configuration, we assume that all FCBs and switches in the feeders electrically connected with the fault section are opened in the first step. Then, the sequential fault detection system controls the switches to identify the fault section and to supply power to the nonfaulted section of each feeder, similar to a radial configuration. In this assumption, the nonsupplied sections

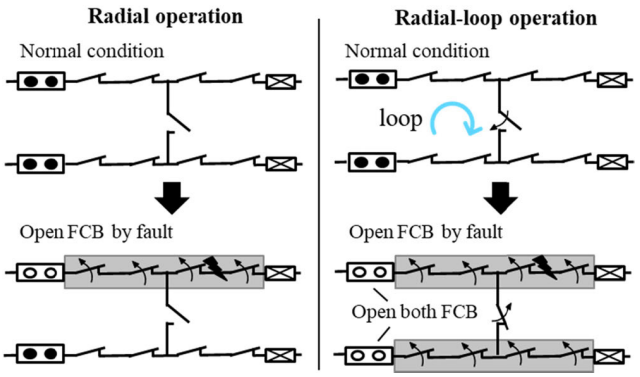

FIGURE 3. Nonsupplied sections created by opening the FCB in a radial operation and in a radial-loop operation. In the radial-loop operation, nonsupplied sections are larger than those in the radial operation.

created by opening the FCB expand in the radial-loop configuration compared with the radial configuration, as shown in Fig. 3. Therefore, the DSOs need to determine the radial-loop configuration based on the evaluation of supply reliability under fault conditions.

III. OPTIMAL RADIAL-LOOP CONFIGURATION OF DISTRIBUTION NETWORK

In this paper, the optimal radial-loop configuration is defined as the configuration that minimizes active power loss while satisfying the constraints of node voltage, thermal capacity, fault current detection through the FCB, nonsupplied sections by opening the FCB, and tie-switch status. The radial-loop configuration is constructed by closing the tie-switches in the base radial configuration and includes partial loop structures to use the sequential fault detection system. Therefore, the radial-loop configuration is determined by optimizing the status of the tie-switches in the base radial configuration without establishing new distribution lines and devices. In addition, it is assumed that DSOs can remotely change the status of the tie-switches [28]. Thus, the expenses are not included in the formulation. The concept of the optimization problem is shown in Fig. 4 and formulated as follows.

A. OBJECTIVE FUNCTION

As given in Eq. (2) and Eq. (3), the objective function is the total active power loss, and the optimal configuration is determined to minimize the index among the configuration candidates $\mathcal{X}_k$, which satisfy the electrical constraints and the tie-switch status constraint, as given in Eq. (4). The configuration candidates $\mathcal{X}_k$ are defined as a vector of the status of tie-switches $SW_{n,k}$ ($SW_{n,k} = 0$: open, $SW_{n,k} = 1$: closed) as given in Eq. (5) and Eq. (6). To explore the optimal configuration, the status of the tie-switches is controlled.

$$\min_{k\in K} \sum\nolimits_{t\in T} loss_t\left(\mathcal{X}_k\right), \tag{2}$$

$$loss_t\left(\mathcal{X}_k\right) = \sum\nolimits_{l\in L} 3\times \sim I_{l,t}^2(\mathcal{X}_k) \times \sim R_l, \quad \forall k \in K, \tag{3}$$

$$\mathcal{X}_k \in (\mathcal{X}^{\text{elec}} \cap \mathcal{X}^{\text{topol}}), \quad \forall k \in K, \tag{4}$$

$$\mathcal{X}_k = \left[SW_{1,k}, SW_{2,k}, \ldots, SW_{n,k}, \ldots, SW_{N,k}\right], \quad \forall k \in K, \tag{5}$$

$$SW_{n,k} \in \{0, 1\}, \quad \forall n \in N, \ \forall k \in K, \tag{6}$$

where $loss_t\left(\mathcal{X}_k\right)$ is the active power loss at verification time step t in configuration $\mathcal{X}_k$, T is the total verification time step of the power flow calculation, $\mathcal{X}_k$ is the k-th configuration candidate, $I_{l,t}\left(\mathcal{X}_k\right)$ is a phase current through distribution line l at verification time step t in configuration $\mathcal{X}_k$, R_l is the resistance of distribution line l, L is the total number of distribution lines, K is the total number of configuration candidates that satisfy the constraints, $\mathcal{X}^{\text{elec}}$ is the set of configurations satisfying the electrical constraints in Eqs. (7)-(14), $\mathcal{X}^{\text{topol}}$ is the set of configurations satisfying the constraint of the tie-switch status in Eq. (15), $SW_{n,k}$ is the status of tie-switch n in configuration $\mathcal{X}_k$ and N is the total number of tie-switches.

B. CONSTRAINTS

The optimization problem includes five constraints relating to the normal condition, fault condition and tie-switch status; 1) node voltage constraint, 2) thermal capacity constraint, 3) constraint for fault current detection by the FCB, 4) constraint for the nonsupplied section by opening the FCB and 5) constraint for the total number of closed tie-switches. In this paper, the fault is assumed to be a short-circuit fault and not a ground fault such as 3-line to ground fault (3LG), because a ground fault can be detected and cleared by the IT-switch operation without opening the FCB in the radial configuration [28], [29]. This procedure is also assumed to apply to the radial-loop configuration. However, the detection and clearing of a short-circuit fault, such as 3-line short circuit fault (3LS) or 2LS, by the IT-switch seems to be difficult because the capacity of the IT-switch is generally not sufficient to clear the short-circuit current. Therefore, this paper assumes a short-circuit fault to evaluate constraints 3) and 4).

1) NODE VOLTAGE CONSTRAINT

This constraint considers that the node voltage is managed within the proper range under normal conditions, as given in Eq. (7),

$$\underline{V} \le V_{m,t}\left(\mathcal{X}_{k'}^{\text{all}}\right) \le \overline{V}, \quad \forall m \in M, \forall t \in T, \tag{7}$$

where $\overline{V}$ and $\underline{V}$ are the upper and lower limits of the node voltage proper range, respectively, and $V_{m,t}\left(\mathcal{X}_{k'}^{\text{all}}\right)$ is the voltage in node m at the verification time step t in the configuration $\mathcal{X}_{k'}^{\text{all}}$, $\mathcal{X}_{k'}^{\text{all}}$ is the k'-th configuration in the set of all configurations by controlling the tie-switch status, K' is the total number of all configurations by controlling the tie-switch status, and M is the total number of nodes with load.

2) THERMAL CAPACITY CONSTRAINT

This constraint considers that the power flow through the distribution line is managed to be lower than the thermal capacity, as given in Eq. (8),

$$I_{l,t}\left(\mathcal{X}_{k'}^{\text{all}}\right) \le \overline{I}_l, \quad \forall l \in L, \ \forall t \in T, \tag{8}$$

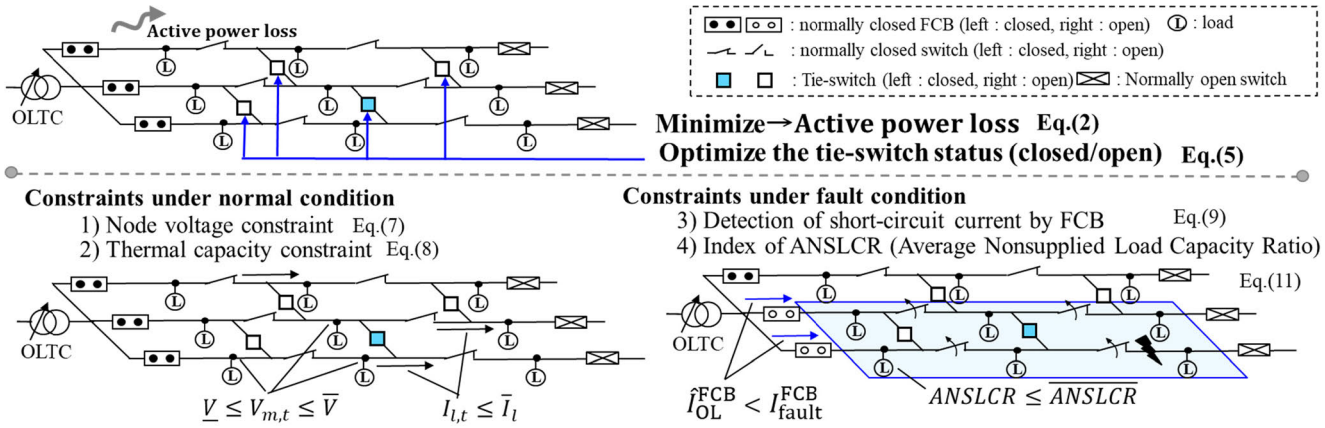

FIGURE 4. Concept of optimal radial-loop configuration. The radial-loop configuration is constructed by closing tie-switches in a base radial configuration. The optimal configuration is determined to minimize active power loss while satisfying the constraints under normal and fault conditions.

where $\overline{I}_l$ is the thermal capacity of the distribution line l and $I_{l,t}\left(\mathcal{X}_{k'}^{\mathrm{all}}\right)$ is a phase current through a distribution line l at the verification time step t in the configuration $\mathcal{X}_{k'}^{\mathrm{all}}$.

If these constraints in Eq. (7) and Eq. (8) are not satisfied due to PV system generation, the PV system generation may be curtailed. Satisfying these constraints is important for not only the management of power quality but also the efficient utilization of PV systems.

3) DETECTION OF SHORT-CIRCUIT CURRENT BY FCB

The detection of a short-circuit current by the FCB is necessary for improving the supply reliability in the radial-loop configuration as described in Section II. The constraint is as given in Eq. (9),

$$\hat{I}_{\mathrm{OL}}^{\mathrm{FCB}}(f) < \min_{p\in P} I_{\mathrm{fault}}^{\mathrm{FCB}}(\mathcal{X}_{k'}^{\mathrm{all}}, p, f), \quad \forall f \in F, \tag{9}$$

$$\hat{I}_{\mathrm{OL}}^{\mathrm{FCB}}(f) = K_{\mathrm{OL}} \times \sim \overline{I}^{FCB}(f), \tag{10}$$

where $\hat{I}_{\mathrm{OL}}^{\mathrm{FCB}}(f)$ is the threshold parameter of current through the FCB in feeder f to detect an overload, K_{OL} is the coefficient for overload detection, $\overline{I}^{FCB}(f)$ is the thermal capacity of the distribution line with the FCB in feeder f, F is the total number of feeders in a substation, $I_{\mathrm{fault}}^{\mathrm{FCB}}(\mathcal{X}_{k'}^{\mathrm{all}}, p, f)$ is the current through an FCB in feeder f in configuration $\mathcal{X}_{k'}^{\mathrm{all}}$ in fault case #p and P is the total number of assumed cases for a short-circuit fault. In each case, the point of the short-circuit fault is different.

The constraint in Eq. (9) indicates that the threshold current for the detection of overload $\hat{I}_{\mathrm{OL}}^{\mathrm{FCB}}(f)$ is lower than the minimum value of the assumed short-circuit current through the FCB in feeder f. Satisfying this constraint indicates that the FCB can detect overload and short-circuit faults properly and that the sequential fault detection system can be applied to the radial-loop configuration. In this paper, the root and the end nodes in each feeder are selected as the locations of short-circuit faults to assume severe conditions for fault current detection by the FCB. A 2LS is assumed to be the fault type because the current decreases more than in a 3LS [28].

4) AVERAGE NONSUPPLIED LOAD CAPACITY RATIO (ANSLCR) CONSTRAINT

As shown in Fig. 3, the supply reliability may deteriorate from the expansion of the nonsupplied section under a fault in the radial-loop configuration. In this paper, the expansion level is defined as the average nonsupplied load capacity ratio (ANSLCR), and the index indicates the ratio of the expansion level against the base radial configuration. The optimal configuration is selected from the configurations where the index is lower than a threshold of the expansion level. The constraint is given in Eq. (11).

$$ANSLCR\left(\mathcal{X}_{k'}^{\mathrm{all}}\right) \le \overline{ANSLCR}, \tag{11}$$

where $ANSLCR(\mathcal{X}_{k'}^{\mathrm{all}})$ is the ANSLCR in the configuration $\mathcal{X}_{k'}^{\mathrm{all}}$ and $\overline{ANSLCR}$ is the upper limit of the index ANSLCR. The procedure used to calculate the index ANSLCR consists of 3 steps, and an overview is shown in Fig. 5 using an example that is a 3-feeder distribution network model. In Step 1, an average nonsupplied load capacity (ANSLC) is calculated for the base radial configuration $ANSLC\left(\mathcal{X}^{\mathrm{radial}}\right)$,

$$ANSLC\left(\mathcal{X}^{\mathrm{radial}}\right) = \frac{\sum_{f\in F} NSLC_f\left(\mathcal{X}^{\mathrm{radial}}\right) \times \sim t_{clear}}{F}, \tag{12}$$

where $NSLC_f(\mathcal{X}^{\mathrm{radial}})$ is the total nonsupplied load capacity (NSLC) in nonfaulted sections from a fault in feeder f in the radial configuration $\mathcal{X}^{\mathrm{radial}}$, as shown in Fig. 5. To consider the uncertainty of fault points simply, the end section of each feeder is assumed to be the fault section, and the average value is used as an index. t_{clear} is the time needed to finish the procedure by the sequential fault detection system and is generally 1 minute. In Step 2, the ANSLC index for a radial-loop configuration $ANSLC\left(\mathcal{X}_{k'}^{\mathrm{all}}\right)$ is calculated by the same procedure in the radial configuration,

$$ANSLC\left(\mathcal{X}_{k'}^{\mathrm{all}}\right) = \frac{\sum_{f\in F} NSLC_f\left(\mathcal{X}_{k'}^{\mathrm{all}}\right) \times \sim t_{clear}}{F}, \quad \forall k' \in K', \tag{13}$$

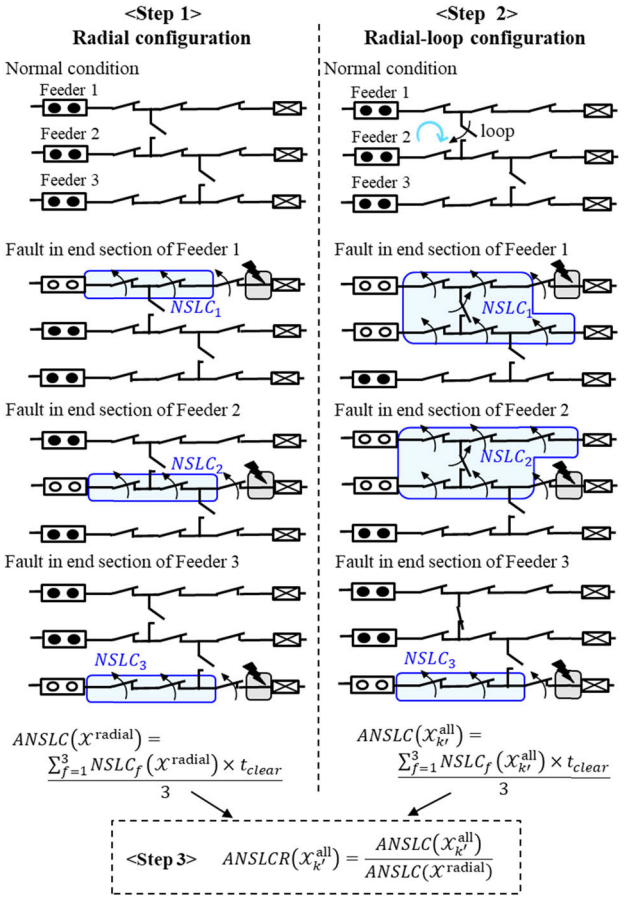

FIGURE 5. Overview of the ANSLCR index calculation. In Step 1 and Step 2, the ANSLC index is calculated for the base radial configuration and radial-loop configuration, respectively. The ANSLC index indicates the average of the NSLC index. NSLC is shown as the blue zone. In Step 3, the ANSLCR index is calculated by the ratio of ANSLC.

where $NSLC_f(\mathcal{X}^{\text{all}}_{k'})$ is the NSLC index created by the fault of feeder f in the configuration $\mathcal{X}^{\text{all}}_{k'}$ and K' is the total number of all configurations created by controlling the tie-switch status. The ANSLC index in a radial-loop configuration is larger than that in a radial configuration, as shown in Fig. 5. In Step 3, the ANSLCR index is calculated for each configuration by Eq. (14),

$$ANSLCR\left(\mathcal{X}^{\text{all}}_{k'}\right) = \frac{ANSLC\left(\mathcal{X}^{\text{all}}_{k'}\right)}{ANSLC(\mathcal{X}^{\text{radial}})}, \quad \forall k' \in K'. \quad (14)$$

In the base radial configuration, the ANSLCR index is 1.0. The supply reliability deteriorates as the index increases. Thus, the index has an upper limit as the constraint given in Eq. (11) in this paper.

5) NUMBER OF CLOSED TIE-SWITCHES CONSTRAINT

The final constraint concerns the total number of closed tie-switches, as given in Eq. (15),

$$\sum\nolimits_{n\in N} SW_{n,k'} \leq \overline{cSW}, \quad (15)$$

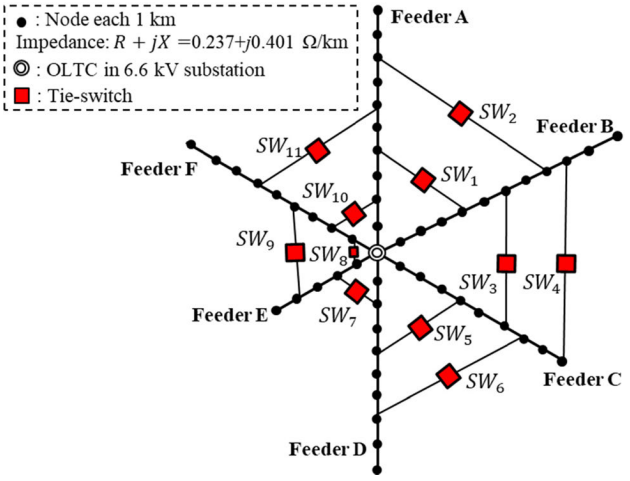

FIGURE 6. A 6.6 kV distribution network model consisting of 6 feeders and 11 tie-switches. This model is constructed based on an existing distribution network in the Kansai area in Japan.

where $\overline{cSW}$ is the upper limit of the total number of closed tie-switches.

An increase in the total number of closed tie-switches can cause additional complexity in power system operation and management. To alleviate this concern, this constraint is used.

IV. NUMERICAL SIMULATION SETTING

A numerical simulation is performed to evaluate the impact on fault detection by using a radial-loop configuration and the effectiveness of the optimal configuration in terms of active power loss and voltage regulation. The settings of the numerical simulation are described as A) a distribution network model, B) parameters, and C) verification cases.

A. DISTRIBUTION NETWORK MODEL

Fig. 6 shows a 6.6 kV distribution network model consisting of 6 feeders and 11 tie-switches. The model is constructed based on an existing distribution network in the Kansai area in Japan. The substation is defined as a constant voltage source that is 77 kV and 60 Hz. An on-load tap changer (OLTC) transforms the voltage from 77 kV to 6.6 kV. Table 1 shows the length and load capacity for each feeder and for each node. The capacity and distribution of the load are different for each feeder. The load and PV systems are defined as a three-phase balanced PQ bus connected to 6.6 kV system. The impedance of all distribution lines between nodes is $0.237 + \text{j}0.401\Omega/\text{km}$. The impedance is defined by the resistance and reactance. The length of the distribution line with tie-switches between feeders is shown in Table 2. The candidates of the configuration are represented by the status of the 11 tie-switches. The tie-switches are defined as a three-phase breaker. The open or closed status is determined by the tie-switch resistance value setting. When the status is open, the resistance is set as a large value to prevent power flow. The resistance is set as almost zero if the status is closed. The network model is constructed in MATLAB/Simulink.

TABLE 1. Settings of the distribution network model.

Contents		Feeder # A	B	C	D	E	F
Length [km]		10	11	9	9	5	9
Total load capacity in Feeder # [kW]		600	600	800	1000	2000	1200
Load capacity in each node [kW] *N1 is a node in the root of a feeder.	N1*	0	0	120	100	200	120
	N2	48	60	0	190	400	120
	N3	0	60	240	170	600	120
	N4	198	0	0	100	200	120
	N5	0	180	80	200	600	240
	N6	78	180	120	60		120
	N7	120	0	120	140		120
	N8	78	0	0	30		120
	N9	0	0	120	10		120
	N10	78	60				
	N11		60				

TABLE 2. Length of distribution lines with tie-switches between feeders.

SW #	Line length	SW #	Line length	SW #	Line length	SW #	Line length
SW_1	4.0 km	SW_4	9.0 km	SW_7	2.0 km	SW_{10}	2.0 km
SW_2	8.0 km	SW_5	4.0 km	SW_8	1.0kn	SW_{11}	6.0 km
SW_3	6.0 km	SW_6	7.0 km	SW_9	4.0 km		

TABLE 3. Parameters under constraints.

Contents	Value
$\underline{V}$	6343 V
$\overline{V}$	6542 V (9.00 hrs-15.00 hrs) 6700 V (0.00 hrs-9.00 hrs and 15.00 hrs-24.00 hrs)
$\overline{I}_l, \forall l \in L$	400 A
K_{OL}	1.7
$\overline{I}^{FCB}(f), \forall f \in F$	400 A
F, P	6, 12
$\overline{ANSLCR}$	2.0
$\overline{cSW}$	6

The power flow calculation is solved by the Newton-Raphson method.

B. PARAMETER SETTINGS

Table 3 shows the parameters relating to the constraints described in Section III. The proper range of node voltages in the 6.6 kV system is determined based on the proper range for low-voltage systems, i.e., 95 V to 107 V [28]. The range is transferred based on a ratio in a pole transformer of 105 V/6600 V. This transformer is general in Japan. The calculated proper range includes a margin allowing for a voltage deviation in the distribution line from the pole transformer to the connection point of the customer. Specifically, the upper limit during the daytime is set as a lower value to consider the voltage rise in a low-voltage system due to PV system generation. The coefficient for overload detection K_{OL} is set based on an actual operation in Japan. The assumed fault points for the short-circuit fault are a root node and an end node in each feeder. The upper limit of the ANSLCR index is determined based on a comparison of the system

TABLE 4. PV system penetration conditions in each case.

Case #	PV system penetration ratio* in each Feeder # [%] A	B	C	D	E	F	Large-scale PV at end of Feeder # B (1.0MW)	A (0.3MW)
1	20	20	20	20	20	20	w/	w/o
2	40	40	20	20	20	40	w/	w/
3	60	60	20	20	20	60	w/	w/
4	80	80	20	20	20	80	w/	w/
5	100	100	20	20	20	100	w/	w/

* PV system penetration ratio represents the ratio of households with PV systems relative to the households in a feeder.

average interruption frequency index (SAIFI) and system average interruption duration index (SAIDI) in Japan as well as those around the world [49]. The ANSLCR index is calculated assuming that a feeder is divided every 2 km by a section switch. The total number of closed tie-switches is limited to 6, which is the minimum number needed to connect all feeders. Additionally, the closing of adjacent tie-switches is prohibited for ease of power flow management. For example, both SW_1 and SW_2 are not simultaneously closed in any configuration. The constraint is given in Eqs. (16)-(20),

$$SW_1 + SW_2 \leq 1, \tag{16}$$
$$SW_3 + SW_4 \leq 1, \tag{17}$$
$$SW_5 + SW_6 \leq 1, \tag{18}$$
$$SW_8 + SW_9 \leq 1, \tag{19}$$
$$SW_{10} + SW_{11} \leq 1. \tag{20}$$

C. VERIFICATION CASES

The effectiveness of the optimal configuration is verified under various penetration levels of the PV systems to consider the transition of PV system penetration. Table 4 shows the PV system penetration settings in each case. The penetration ratio of the PV systems increases from Case 1 to Case 5. The penetration ratio represents the ratio of households with PV systems relative to the households in a feeder [50]. The PV penetration ratio of 100% indicates that all households in a feeder have PV systems. The condition is assumed to be a future power system. In this simulation, the number of households is defined assuming that the load capacity and PV system capacity in each household are 2.0 kW and 3.0 kW, respectively. For example, the total number of households in Feeder A is 300. If the PV penetration ratio is 20%, the number of households with PV systems is 60, and the total PV capacity is 180 kW. The ratio and distribution of PV system penetration are different among the feeders. The PV penetration ratio increases in Feeders A, B and F, as shown in Table 4. In Feeders A and D, the PV systems are installed from the root node to the end node. In Feeders B and E, the PV systems are installed from the end node to the root node. In Feeders C and F, the PV systems are installed into each node at the same ratio.

A power flow calculation is performed to evaluate active power loss and voltage regulation over 2 days during the

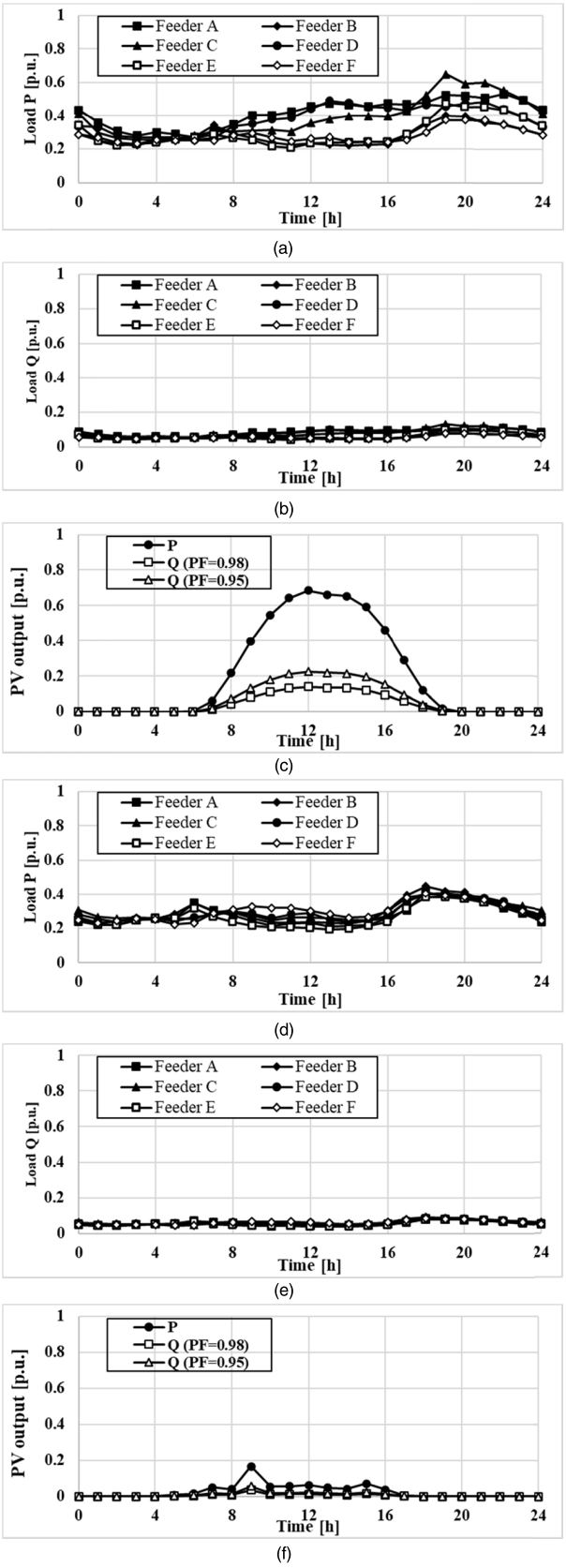

FIGURE 7. Load and PV profiles. (a, b) Active and reactive power profile of load on a sunny day. (c) PV profile on a sunny day. (d, e) Active and reactive power profile of load on a rainy day. (f) PV profile on a rainy day.

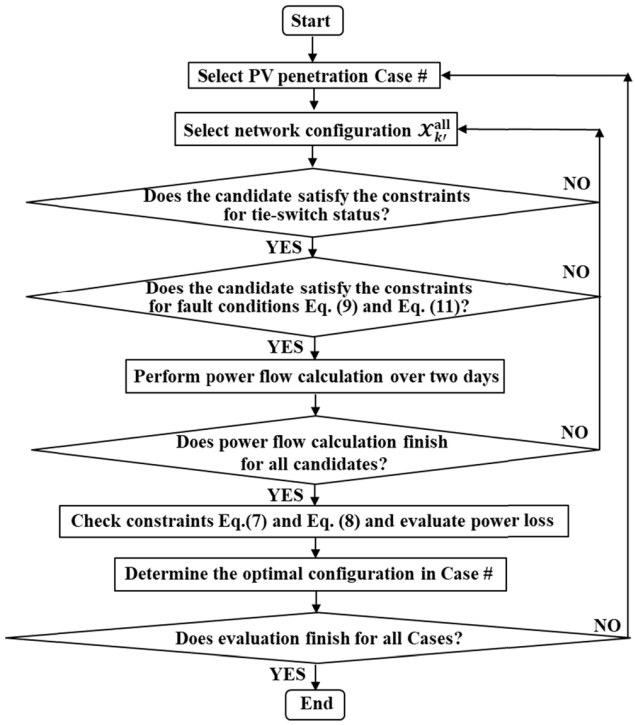

FIGURE 8. Flow of verification.

summer: a sunny day and a rainy day. Fig. 7 shows profiles of the load and generation from the PV system, and these two days are selected randomly from sunny and rainy days during the summer [51]. The time step is 1 hour. This paper focuses on summer because this season has a heavy load demand in Japan and the power system operators adjust the network configuration for each season [52]. Additionally, sunny and rainy days are selected as verification days to consider the generation from PV systems [50].

The method of voltage regulation consists of the tap operation of OLTC in a substation and the reactive power control of the PV systems. The tap of the OLTC is lowered at 08.00 hrs and raised at 16.00 hrs on both days. PV systems generate reactive power based on fixed power factor control [53]. The power factors of the PV systems in households and large-scale PV systems at the ends of Feeders A and B are 0.98 and 0.95, respectively.

Fig. 8 shows the verification procedure. The optimal configuration is determined in each case based on an exhaustive search by controlling the tie-switch status.

V. RESULTS AND DISCUSSION

This section evaluates the impact of an FCB on the detection of short-circuit current in a radial-loop configuration. Then, the effectiveness of the optimal configuration is verified based on active power loss and voltage regulation.

Table 5 shows the total number of configurations satisfying the constraints for the tie-switch status in Eqs. (15)-(20) and the total number of configurations satisfying the constraints

TABLE 5. Total number of configuration candidates satisfying constraints for tie-switch status in Eqs. (15)-(20) and Eq. (9).

Total number of CLOSED tie-switches	Satisfying the constraints of tie-switch status in Eqs. (15)-(20)	Satisfying the constraints of tie-switched status in Eqs. (15)-(20) and Eq. (9)
0 (Radial)	1	1
1	11	11
2	50	48
3	120	83
4	160	35
5	112	0
6	32	1
Total	486	179

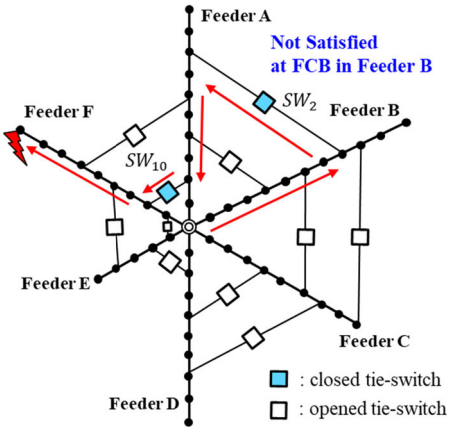

FIGURE 9. Example of a configuration NOT satisfying the constraint in Eq. (9) for total number of closed tie-switches 2. In this configuration, the FCB at the root of Feeder B cannot detect the short-circuit current caused by a fault in the end node of Feeder F.

for the tie-switch status and the detection of short-circuit current in Eq. (9). The value is summarized in each total number of closed tie-switches. The number in the right column decreases compared with the number in the center column because some configuration candidates do not satisfy the constraint in Eq. (9). When the total number of closed tie-switches is greater than two, some candidates cannot satisfy the constraint in Eq. (9). Fig. 9 shows an example of a configuration not satisfying Eq. (9). In the configuration, tie-switches SW_2 and SW_{10} are closed. The FCB in Feeder B cannot detect the short-circuit current by the fault at an end node of Feeder F because the impedance from the FCB to the fault point increases, as shown by the red arrows in Fig. 9. The number of configurations not satisfying the constraint in Eq. (9) increases as the total number of closed tie-switches increases. All configurations do not satisfy Eq. (9) for the case when the total number of closed tie-switches is five. This is because the distribution network model has six feeders, and all the feeders are connected by closing five tie-switches. Therefore, it is important to evaluate the detection of a short-circuit current by the FCB.

The effectiveness of the optimal radial-loop configuration is described for each case as follows. Fig. 10 shows the relationship between the ANSLCR index and active power loss in Case 1. The total number of plots in Fig. 10 is 179, as described in Table 5. The plots on the yellow

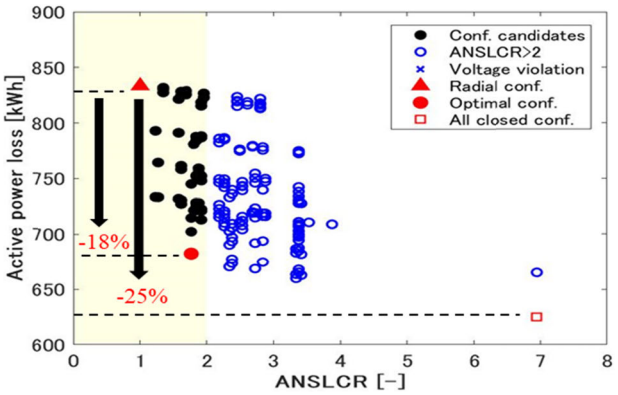

FIGURE 10. Relationship between active power loss and the ANSLCR index in Case 1. In this graph, the area with a yellow background indicates that the ANSLCR is lower than 2.0. The result of the optimal configuration is marked with a red circle, and that of the radial configuration is marked with a red triangle.

background area are the candidates for the optimal configuration. The blue circles represent the indices of configurations not satisfying the constraint for the ANSLCR index, and the red square shows the indices of the configuration where all tie-switches are closed. These indices are shown as references, although the configurations do not satisfy the constraints. The optimal configuration with minimal active power loss is shown with a red circle on the yellow background. The optimal configuration is determined by the same procedure in each case. The active power loss is reduced by 18% against a radial configuration using the optimal configuration. The active power loss in the configuration candidates, shown as black circles, are varied. Some configurations show almost the same active power loss as the radial configuration. Additionally, some configuration candidates deteriorate the ANSLCR index more than the optimal configuration. Therefore, the importance of optimizing the tie-switch status is revealed by these results. The configuration that closes all tie-switches reduces the active power loss by 25% compared to that in the radial configuration. However, the ANSLCR index deteriorates by approximately seven times compared to that in the radial configuration. On the other hand, the optimal configuration reduces the active power loss by 18%, and the ANSLCR index is lower than 2. Specifically, the proposed method can determine the useful configuration that reduces the active power loss without a significant deterioration of the ANSLCR index. According to Fig. 10, there is a trade-off relationship between active power loss and the ANSLCR index. Therefore, the optimal configuration can also be determined by Pareto optimization based on these indices [54]. In that method, the priority between the active power loss and the ANSLCR index can be determined by DSOs.

Next, active power loss and optimal configuration are discussed for each case. Fig. 11 shows the active power loss of the radial configuration and the optimal configuration. Table 6 shows the closed tie-switches of the optimal configuration. In all cases, the optimal configuration can reduce the active power loss by approximately 17% against the radial

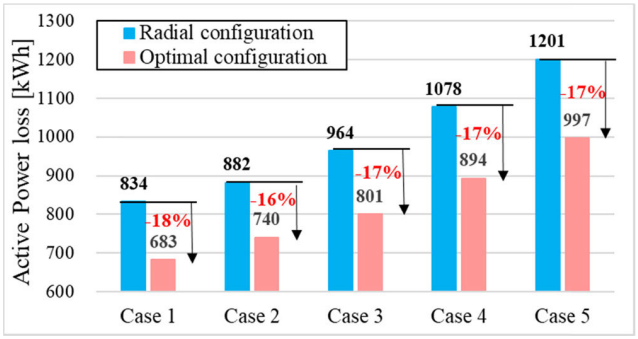

FIGURE 11. Active power loss of radial configuration and optimal configuration for each case.

TABLE 6. Optimal configuration for each case.

Case #	Closed tie-switches	Case #	Closed tie-switches
Case 1	SW_2, SW_4	Case 4	SW_4, SW_6
Case 2	SW_4, SW_6	Case 5	SW_4, SW_9
Case 3	SW_4, SW_6		

configuration, as shown in Fig. 11. This result suggests that the radial-loop configuration is useful under various PV system penetration conditions. In Table 6, the closed tie-switches in the optimal configuration are changed by the transition of PV system penetration. This result suggests that a reconfiguration considering the condition of PV system penetration is useful in reducing active power loss.

To assess the reduction of active power loss and the transition of the optimal configuration, the active power loss in each distribution line is visualized for Cases 1, 2 and 5 in Figs. 12, 13 and 14, respectively. These figures show the active power loss in the radial configuration and the optimal configuration. Each distribution line is colored based on the amount of total active power loss occurring during the verification days. The total active power loss in each feeder is also described. In Fig. 12 (a), the active power loss in Feeder B with large PV systems is largest among feeders in the radial configuration for Case 1. In the optimal configuration, the tie-switches SW_2 and SW_4 are closed, as shown in Fig. 12 (b). The active power loss in Feeder B is significantly reduced by sharing the generation from a large-scale PV system in an end node of Feeder B with Feeders A and C. In Fig. 12 (a), the active power loss in Feeder E is also large. However, the tie-switches connected with Feeder E are not closed. This is because of the similarity of Feeders D, E and F. The PV penetration ratios of these feeders are all 20% in Case 1. Therefore, the partial loop with Feeder E cannot reduce active power loss significantly.

In Case 2, the optimal configuration is changed from that in Case 1. The SW_6 is closed instead of SW_2, as shown in Fig. 13 (b). This is because Feeder A and Feeder B have a large-scale PV, and the contribution of loss reduction by connecting Feeder A and B is small. Compared with Fig. 13 (a) and (b), the active power loss in Feeders B, C, and D is reduced by closing the tie-switches SW_4 and SW_6. The

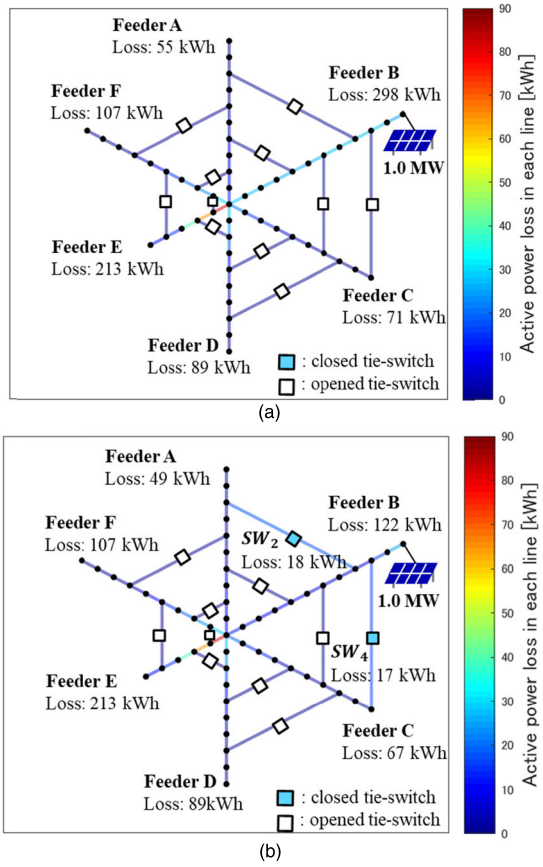

FIGURE 12. Active power loss in each distribution line for Case 1. (a) Radial configuration. (b) Optimal configuration.

loss in Feeder B is almost halved because of the loss reduction in the distribution lines in the roots of Feeder B. Additionally, the loss in Feeder D is reduced by 12 kWh.

In Case 5, the active power loss in Feeders A, B and F increases in the radial configuration due to the increase in PV penetration, as shown in Fig. 14 (a). The optimal configuration is changed from the one in Cases 2-4, and the tie-switch SW_9 is closed instead of SW_6, as shown in Fig. 14 (b). This is because the penetration ratio of PV systems for Feeders A, B and F is 100%, and that for Feeders C, D and E is 20%. The effect of loss reduction increases when connecting with Feeder E and Feeder F. According to Table 1, the load capacity of Feeder E is the largest among the feeders. Compared with Fig. 14 (a) and (b), the active power loss in Feeder B is almost halved by the optimal configuration, although the loss in Feeder C increases by 21 kWh in the optimal configuration. The losses in Feeder E and Feeder F are both reduced by approximately 25 kWh by closing the tie-switch SW_9.

To compare the optimal configuration and other configurations, Table 7 shows the active power loss for three configurations, which were selected as the optimal configuration for each case. This table represents the importance of adjusting the configuration while considering PV system penetration. In Case 2, the active power loss of the optimal configuration in Case 1 and Cases 2-4 are almost the same, at 743 kWh

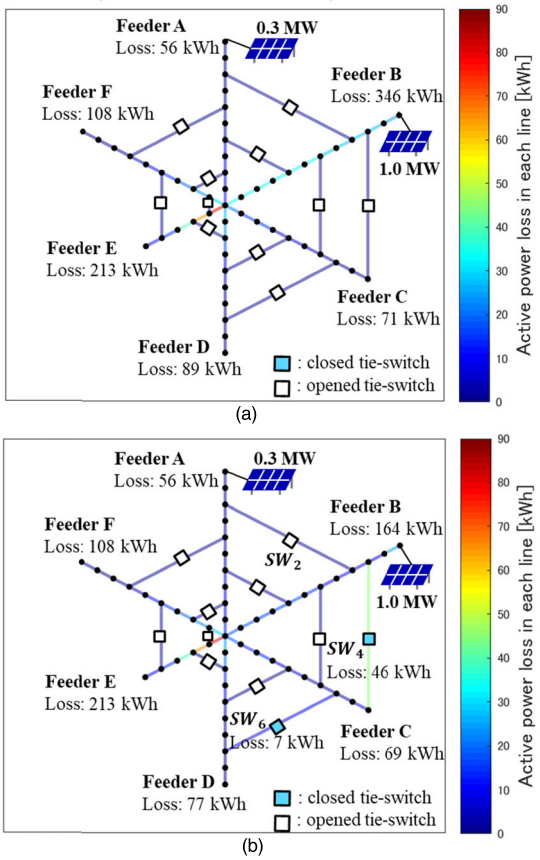

FIGURE 13. Active power loss in each distribution line for Case 2. (a) Radial configuration. (b) Optimal configuration.

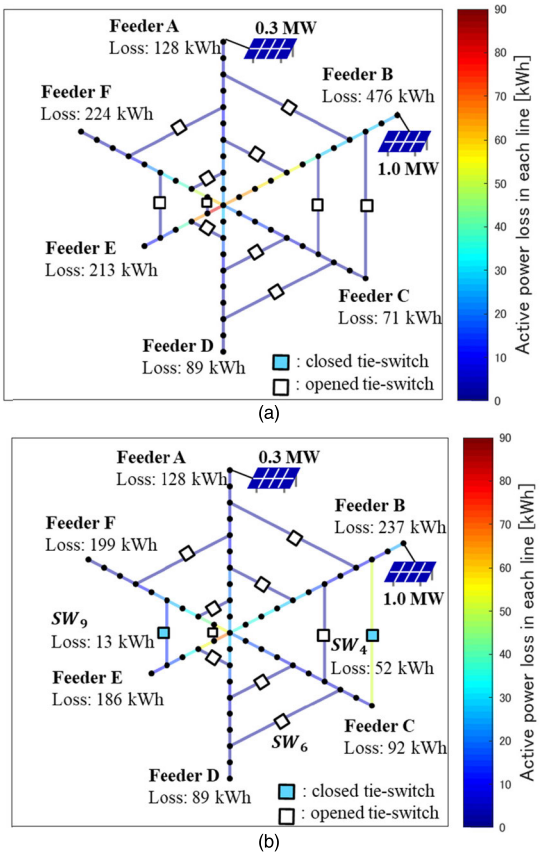

FIGURE 14. Active power loss in each distribution line for Case 5. (a) Radial configuration. (b) Optimal configuration.

TABLE 7. Active power loss of optimal configuration for each case.

Case #	Optimal configuration*		
	Case 1	Case 2-Case 4	Case 5
Case 1	**683**	713	725
Case 2	743	**740**	755
Case 3	810	**801**	813
Case 4	910	**894**	898
Case 5	1031	1006	**997**

* minimum value in each case is written in bold

TABLE 8. Checking node voltage constraint.

Case #	Radial	Optimal	Case #	Radial	Optimal
Case 1	✓	✓	Case 4	✗	✓
Case 2	✓	✓	Case 5	✗	✓
Case 3	✗	✓			

and 740 kWh, respectively. However, the difference in the power loss between these configurations is larger in Case 4. These differences affect the operation as an integrated value. Therefore, the configuration needs to be adjusted to minimize power loss while considering PV system penetration.

Additionally, the radial-loop configuration can contribute to voltage regulation. Table 8 shows the existence of a voltage violation in a radial configuration and the optimal configuration for each case. The voltage violation is caused by generation from PV systems in the radial configuration in Cases 3 to 5. However, the voltage violation is cleared in the optimal configurations. Fig. 15 shows the voltage profiles on the sunny day in Case 4. The node voltages are colored based on feeders. The voltage violation occurs at the node in Feeder B during the daytime in the radial configuration. The OLTC cannot clear the voltage violation because the tap drop causes the voltage violation from the lower limit in Feeder D.

Therefore, generation from PV systems may need to be curtailed to manage node voltages within the proper range. The curtailment of PV system generation should be avoided because a loss of generation opportunity is created. In the optimal radial-loop configuration, the voltage violation is cleared by sharing the generation from PV systems with Feeders C and D, as shown in Fig. 15 (b). This result indicates that the optimal radial-loop configuration can accept more PV systems without voltage violation and curtailment. Additionally, the voltage drop in Feeder D during the daytime is mitigated in the optimal configuration compared with the profiles in the radial configuration, as shown in Fig. 15. In particular, the widths between the maximum and minimum node voltages at 13.00 hrs are 202 V and 130 V in the radial configuration and the optimal configuration, respectively. The voltage width is mitigated by approximately 36%. This result suggests a contribution to the voltage regulation by the radial-loop configuration. Additionally, the mitigation of voltage width contributes to the reduction of the reactive

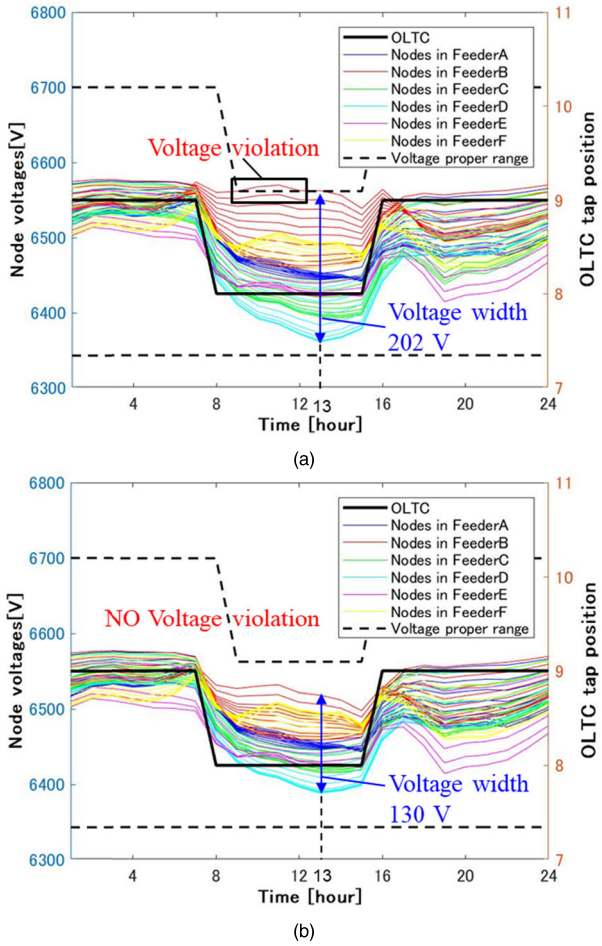

FIGURE 15. Voltage profile on a sunny day in Case 4. (a) Radial configuration. (b) Optimal configuration.

power required from distributed generators and capacitor banks for managing voltage conditions [55]. As the reactive power required for voltage management is reduced, the scale of the capacitor bank is reduced, and economic investment in the power system is expected.

According to these results and analysis, this paper has shown the impact of the detection of short-circuit current by FCBs in the radial-loop configuration and the effectiveness of the optimal configuration based on active power loss and voltage regulation.

VI. CONCLUSION

This paper proposes a method to determine the optimal radial-loop configuration for future power system operations utilizing existing equipment and systems without installing new equipment. The radial-loop configuration includes a partial loop structure by closing the tie-switches in the base radial configuration. This configuration can be applied easily to distribution network operations in terms of the switch operation, and the sequential fault detection system can be used like the operation in a radial configuration. In the proposed method, an optimal configuration is achieved by minimizing active power loss while satisfying the constraints relating to the normal condition, fault condition and tie-switch status. In a numerical simulation, the impact on fault detection by an FCB in a radial-loop configuration is evaluated, and the importance of this evaluation is demonstrated. Then, the effectiveness of the optimal radial-loop configuration is evaluated based on active power loss and voltage regulation under several conditions of PV system penetration. The active power loss is reduced by approximately 17% compared to a radial configuration. The voltage violation in the radial configuration is cleared by using the optimal radial-loop configuration. Additionally, the necessity to adjust the configuration is suggested by considering PV system penetration. These results indicate that the radial-loop configuration can reduce power loss while accepting more PV systems in terms of voltage regulation. It is thus considered that the radial-loop configuration is a useful scheme for achieving a sustainable society with future power system operations.

In this paper, a numerical simulation is performed that focuses on a sunny day and a rainy day during the summer under several cases of PV system penetration, and the load profiles are fixed in each PV penetration case. To evaluate the effectiveness of the radial-loop configuration in detail, the simulation is performed while assuming various days and scenarios considering the electric needs of the consumers, such as installing electric vehicles. Thus, our future work will evaluate the effectiveness of the radial-loop configuration based on annual verification under various scenarios. In addition, the voltage regulation scheme of the OLTC and the cooperation with other devices in the radial-loop configuration will be verified.

REFERENCES

[1] B. Sultana, M. W. Mustafa, U. Sultana, and A. R. Bhatti, "Review on reliability improvement and power loss reduction in distribution system via network reconfiguration," *Renew. Sustain. Energy Rev.*, vol. 66, pp. 297–310, Dec. 2016.

[2] M. S. Ali, M. M. Haque, and P. Wolfs, "A review of topological ordering based voltage rise mitigation methods for LV distribution networks with high levels of photovoltaic penetration," *Renew. Sustain. Energy Rev.*, vol. 103, pp. 463–476, Apr. 2019.

[3] United Nations Climate Change. (2015). *COP21-Decisions*. [Online]. Available: https://unfccc.int/process-and-meetings/conferences/past-conferences/paris-climate-change-conference-november-2015/cop-21/cop-21-decisions

[4] M. Ventosa, Á. Baıllo, A. Ramos, and M. Rivier, "Electricity market modeling trends," *Energy Policy*, vol. 33, no. 7, pp. 897–913, May 2005.

[5] M. O. Buygi, H. M. Shanechi, G. Balzer, M. Shahidehpour, and N. Pariz, "Network planning in unbundled power systems," *IEEE Trans. Power Syst.*, vol. 21, no. 3, pp. 1379–1387, Aug. 2006.

[6] Ministry of Economy, Trade and Industry, Electricity and Gas Market Reform Office Agency for Natural Resources and Energy (ANRE). (2015). *Japan's Electricity Market Deregulation*. [Online]. Available: https://www.meti.go.jp/english/policy/energy_environment/electricity_system_reform/pdf/201506EMR_in_Japan.pdf

[7] B. Mukhopadhyay and D. Das, "Multi-objective dynamic and static reconfiguration with optimized allocation of PV-DG and battery energy storage system," *Renew. Sustain. Energy Rev.*, vol. 124, May 2020, Art. no. 109777.

[8] R. Rajaram, K. Sathish Kumar, and N. Rajasekar, "Power system reconfiguration in a radial distribution network for reducing losses and to improve voltage profile using modified plant growth simulation algorithm with distributed generation (DG)," *Energy Rep.*, vol. 1, pp. 116–122, Nov. 2015.

[9] R. S. Rao, K. Ravindra, K. Satish, and S. V. L. Narasimham, "Power loss minimization in distribution system using network reconfiguration in the presence of distributed generation," *IEEE Trans. Power Syst.*, vol. 28, no. 1, pp. 317–325, Feb. 2013.

[10] T. Tran The, D. Vo Ngoc, and N. Tran Anh, "Distribution network reconfiguration for power loss reduction and voltage profile improvement using chaotic stochastic fractal search algorithm," *Complexity*, vol. 2020, pp. 1–15, Mar. 2020.

[11] D. Das, "A fuzzy multiobjective approach for network reconfiguration of distribution systems," *IEEE Trans. Power Del.*, vol. 21, no. 1, pp. 202–209, Jan. 2006.

[12] P. Kumar, I. Ali, M. S. Thomas, and S. Singh, "A coordinated framework of DG allocation and operating strategy in distribution system for configuration management under varying loading patterns," *Electr. Power Compon. Syst.*, vol. 48, nos. 1–2, pp. 1–18, 2020.

[13] K. Sathish Kumar and T. Jayabarathi, "Power system reconfiguration and loss minimization for an distribution systems using bacterial foraging optimization algorithm," *Int. J. Electr. Power Energy Syst.*, vol. 36, no. 1, pp. 13–17, Mar. 2012.

[14] M. R. Dorostkar-Ghamsari, M. Fotuhi-Firuzabad, M. Lehtonen, and A. Safdarian, "Value of distribution network reconfiguration in presence of renewable energy resources," *IEEE Trans. Power Syst.*, vol. 31, no. 3, pp. 1879–1888, May 2016.

[15] W. Zheng, W. Huang, and D. J. Hill, "A deep learning-based general robust method for network reconfiguration in three-phase unbalanced active distribution networks," *Int. J. Electr. Power Energy Syst.*, vol. 120, Sep. 2020, Art. no. 105982.

[16] M. R. Narimani, R. Azizipanah-Abarghooee, M. Javidsharifi, and A. A. Vahed, "Enhanced gravitational search algorithm for multi-objective distribution feeder reconfiguration considering reliability, loss and operational cost," *IET Gener., Transmiss. Distrib.*, vol. 8, no. 1, pp. 55–69, Jan. 2014.

[17] Y.-Y. Hong and S.-Y. Ho, "Determination of network configuration considering multiobjective in distribution systems using genetic algorithms," *IEEE Trans. Power Syst.*, vol. 20, no. 2, pp. 1062–1069, May 2005.

[18] V. Fathi, H. Seyedi, and B. M. Ivatloo, "Reconfiguration of distribution systems in the presence of distributed generation considering protective constraints and uncertainties," *Int. Trans. Electr. Energy Syst.*, vol. 30, no. 5, pp. 1–25, May 2020.

[19] A. Mohamed Imran and M. Kowsalya, "A new power system reconfiguration scheme for power loss minimization and voltage profile enhancement using fireworks algorithm," *Int. J. Electr. Power Energy Syst.*, vol. 62, pp. 312–322, Nov. 2014.

[20] B. Khorshid-Ghazani, H. Seyedi, B. Mohammadi-ivatloo, K. Zare, and S. Shargh, "Reconfiguration of distribution networks considering coordination of the protective devices," *IET Gener., Transmiss. Distrib.*, vol. 11, no. 1, pp. 82–92, Jan. 2017.

[21] D.-L. Duan, X.-D. Ling, X.-Y. Wu, and B. Zhong, "Reconfiguration of distribution network for loss reduction and reliability improvement based on an enhanced genetic algorithm," *Int. J. Electr. Power Energy Syst.*, vol. 64, pp. 88–95, Jan. 2015.

[22] N. Gupta, A. Swarnkar, and K. R. Niazi, "Distribution network reconfiguration for power quality and reliability improvement using genetic algorithms," *Int. J. Electr. Power Energy Syst.*, vol. 54, pp. 664–671, Jan. 2014.

[23] P. Pavani and S. N. Singh, "Reconfiguration of radial distribution networks with distributed generation for reliability improvement and loss minimization," in *Proc. IEEE Power Energy Soc. Gen. Meeting*, 2013, pp. 31–35.

[24] B. Amanulla, S. Chakrabarti, and S. N. Singh, "Reconfiguration of power distribution systems considering reliability and power loss," *IEEE Trans. Power Del.*, vol. 27, no. 2, pp. 918–926, Apr. 2012.

[25] A. Kavousi-Fard, T. Niknam, and M. Fotuhi-Firuzabad, "Stochastic reconfiguration and optimal coordination of V2G plug-in electric vehicles considering correlated wind power generation," *IEEE Trans. Sustain. Energy*, vol. 6, no. 3, pp. 822–830, Jul. 2015.

[26] T. Yip, B. Xu, Z. Zhu, Y. Chen, and C. Brunner, "Application of IEC 61850 for distribution network automation with distributed control," *J. Eng.*, vol. 2018, no. 15, pp. 993–996, Oct. 2018.

[27] T. Amau, K. Kojima, Y. Saka, Y. Saiki, T. Otani, K. Nishiwaki, M. Aoki, and H. Ukai, "A next-generation distribution automation system using IEC 61850 GOOSE and section switches with sensors," *Electr. Eng. Jpn.*, vol. 195, no. 2, pp. 21–34, Apr. 2016.

[28] Electric Technology Research Association, "Advancement of distribution automation system technology," (in Japanese), *Denkikyoudoukenkyu*, vol. 72, no. 3, 2016.

[29] A. Fujisawa, "Oversea distribution automation system based on japanese experiences," in *Proc. 6th Int. Conf. Adv. Power Syst. Control, Oper. Management.*, 2003, pp. 479–484.

[30] J. Xiao, Y. Wang, F. Luo, L. Bai, F. Gang, R. Huang, X. Jiang, and X. Zhang, "Flexible distribution network: Definition, configuration, operation, and pilot project," *IET Gener., Transmiss. Distrib.*, vol. 12, no. 20, pp. 4492–4498, Nov. 2018.

[31] X. Xing, J. Lin, C. Wan, and Y. Song, "Model predictive control of LPC-looped active distribution network with high penetration of distributed generation," *IEEE Trans. Sustain. Energy*, vol. 8, no. 3, pp. 1051–1063, Jul. 2017.

[32] W. Wang, S. Jazebi, F. de Leon, and Z. Li, "Looping radial distribution systems using superconducting fault current limiters: Feasibility and economic analysis," *IEEE Trans. Power Syst.*, vol. 33, no. 3, pp. 2486–2495, May 2018.

[33] N. Okada, "A method to determine the distributed control setting of looping devices for active distribution systems," in *Proc. IEEE Bucharest PowerTech*, Jun. 2009, pp. 1–6.

[34] N. Okada, "Verification of control method for a loop distribution system using loop power flow controller," in *Proc. IEEE PES Power Syst. Conf. Expo.*, Oct. 2006, pp. 2116–2123.

[35] M. A. Sayed and T. Takeshita, "Line loss minimization in isolated substations and multiple loop distribution systems using the UPFC," *IEEE Trans. Power Electron.*, vol. 29, no. 11, pp. 5813–5822, Jan. 2014.

[36] M.-C. Alvarez-Herault, N. N'Doye, C. Gandioli, N. Hadjsaid, and P. Tixador, "Meshed distribution network vs reinforcement to increase the distributed generation connection," *Sustain. Energy, Grids Netw.*, vol. 1, pp. 20–27, Mar. 2015.

[37] F. R. Islam, K. Prakash, K. A. Mamun, A. Lallu, and H. R. Pota, "Aromatic network: A novel structure for power distribution system," *IEEE Access*, vol. 5, pp. 25236–25257, 2017.

[38] M. Nijhuis, M. Gibescu, and S. Cobben, "Risk-based framework for the planning of low-voltage networks incorporating severe uncertainty," *IET Gener., Transmiss. Distrib.*, vol. 11, no. 2, pp. 419–426, Jan. 2017.

[39] J.-C. Kim, S.-M. Cho, and H.-S. Shin, "Advanced power distribution system configuration for smart grid," *IEEE Trans. Smart Grid*, vol. 4, no. 1, pp. 353–358, Mar. 2013.

[40] S. Ahmad, M. J. Afzal, and S. A. A. Kazmi, "Comparative analysis of radial and looped distribution network against voltage stability and loadability with distributed generation," in *Proc. 5th Int. Symp. Environ.-Friendly Energies Appl. (EFEA)*, Sep. 2018, pp. 1–6.

[41] M.-C. Alvarez-Herault, D. Picault, R. Caire, B. Raison, N. HadjSaid, and W. Bienia, "A novel hybrid network architecture to increase DG insertion in electrical distribution systems," *IEEE Trans. Power Syst.*, vol. 26, no. 2, pp. 905–914, May 2011.

[42] A. Navarro-Espinosa, L. F. Ochoa, and D. Randles, "Assessing the benefits of meshed operation of LV feeders with low carbon technologies," in *Proc. ISGT*, Feb. 2014, pp. 1–5.

[43] A. Zidan and E. F. El-Saadany, "Effect of network configuration on maximum loadability and maximum allowable DG penetration in distribution systems," in *Proc. IEEE Electr. Power Energy Conf.*, Aug. 2013, pp. 1–6.

[44] G. Celli, F. Pilo, G. Pisano, R. Cicoria, and A. Iaria, "Meshed vs. Radial MV distribution network in presence of large amount of DG," in *Proc. IEEE PES Power Syst. Conf. Expo.*, Oct. 2004, pp. 709–714.

[45] A.-E. Hamad, A. Hoballah, and A. M. Azmy, "Defining optimal DG penetration for minimizing energy losses concerning repairing fault periods," in *Proc. 18th Int. Middle East Power Syst. Conf. (MEPCON)*, Dec. 2016, pp. 1–6.

[46] S. A. A. Kazmi and D. R. Shin, "DG placement in loop distribution network with new voltage stability index and loss minimization condition based planning approach under load growth," *Energies*, vol. 10, no. 8, pp. 1–28, 2017.

[47] Z. Yang, Y. Li, and J. Xiang, "Coordination control strategy for power management of active distribution networks," *IEEE Trans. Smart Grid*, vol. 10, no. 5, pp. 5524–5535, Sep. 2019.

[48] M. Wittenstein. (2018). *International Perspectives on Electricity System Resilience*. [Online]. Available: https://www.meti.go.jp/shingikai/enecho/denryoku_gas/denryoku_gas/pdf/014_03_02.pdf

[49] The Organization for Cross-regional Coordination of Transmission Operators (OCCTO), JAPAN. (2018). *Report on the Quality of Electricity Supply*. [Online]. Available: https://www.occto.or.jp/en/information_disclosure/miscellaneous/files/181221_qualityofelectoricity_2017.pdf

[50] S. Akagi, R. Takahashi, A. Kaneko, M. Ito, J. Yoshinaga, Y. Hayashi, H. Asano, and H. Konda, "Upgrading voltage control method based on photovoltaic penetration rate," *IEEE Trans. Smart Grid*, vol. 9, no. 5, pp. 3994–4003, Sep. 2018.
[51] (2009). *New Energy and Industrial Technology Development Organization*. [Online]. Available: https://www.nedo.go.jp/library/seika/shosai_200910/20090000000504.html
[52] C.-S. Chen and M.-Y. Cho, "Energy loss reduction by critical switches," *IEEE Trans. Power Del.*, vol. 8, no. 3, pp. 1246–1253, Jul. 1993.
[53] P. Chaudhary and M. Rizwan, "Voltage regulation mitigation techniques in distribution system with high PV penetration: A review," *Renew. Sustain. Energy Rev.*, vol. 82, pp. 3279–3287, Feb. 2018.
[54] A. Asrari, S. Lotfifard, and M. S. Payam, "Pareto dominance-based multiobjective optimization method for distribution network reconfiguration," *IEEE Trans. Smart Grid*, vol. 7, no. 3, pp. 1401–1410, May 2016.
[55] K. Mahmoud and M. Lehtonen, "Simultaneous allocation of multi-type distributed generations and capacitors using generic analytical expressions," *IEEE Access*, vol. 7, pp. 182701–182710, 2019.

AKIHISA KANEKO (Graduate Student Member, IEEE) received the B.Eng. and M.Eng. degrees in electrical engineering and bioscience from Waseda University, Tokyo, Japan, in 2016 and 2018, respectively, where he is currently pursuing the Ph.D. degree in electrical power engineering. His research interests include the cooperative control of renewable energy sources in distribution and transmission systems.

YASUHIRO HAYASHI (Member, IEEE) received the B.Eng., M.Eng., and D.Eng. degrees from Waseda University, Tokyo, Japan, in 1989, 1991, and 1994, respectively. In 1994, he became a Research Associate with Ibaraki University, Mito, Japan. In 2000, he became an Associate Professor with the Department of Electrical and Electronics Engineering, Fukui University, Fukui, Japan. He has been with a Professor with the Department of Electrical Engineering and Bioscience, Waseda University, since 2009, where has been the Director with the Research Institute of Advanced Network Technology since 2010. Since 2014, he has been the Dean of the Advanced Collaborative Research Organization for Smart Society at Waseda University. His current research interests include the optimization of distribution system operation and forecasting, operation, planning, and control concerned with renewable energy sources and demand responses. He is a member of the Institute of Electrical Engineers of Japan and a Regular Member of CIGRE SC C6 (Distribution Systems and Dispersed Generation).

TAKAYA ANEGAWA received the M.Eng. degree from Ritsumeikan University, Japan, in 2009. He joined Kansai Transmission and Distribution, Inc. (formerly Kansai Electric Power Company, Inc.), in 2009. He is in charge of the development of distribution automation systems.

HIDEYASU HOKAZONO received the M.Eng. degree from Waseda University, Japan, in 2000. He joined Kansai Transmission and Distribution, Inc. (formerly Kansai Electric Power Company, Inc.), in 2000. He is in charge of the development of distribution automation systems.

YUKIYASU KUWASHITA received the M.Eng. degree from Nagoya University, Japan, in 1996. He joined Kansai Transmission and Distribution, Inc. (formerly Kansai Electric Power Company, Inc.), in 1996. He is in charge of the development of distribution automation systems and smart meters.